MOX-Report No. 41/2018

The role of near-field ground motion on seismic risk assessment in large urban areas

Mazzieri, I.; Melas, L.; Smerzini, C.; Stupazzini, M.

MOX, Dipartimento di Matematica
Politecnico di Milano, Via Bonardi 9 - 20133 Milano (Italy)

mox-dmat@polimi.it http://mox.polimi.it

THE ROLE OF NEAR-FIELD GROUND MOTION ON SEISMIC RISK ASSESSMENT IN LARGE URBAN AREAS

Ilario MAZZIERI[1], Laura MELAS[2], Chiara SMERZINI[3], Marco STUPAZZINI[4]

ABSTRACT

During the last ten years a long series of events like Wenchuan (2008, China), l'Aquila (Italy, 2009), Christchurch (New Zealand, 2010-2011), Emilia-Romagna (Italy, 2012), Meinong (Taiwan, 2016), Kumamoto (Japan, 2016) and Norcia (Italy, 2016) once more proved that the near-field of an earthquake poses a serious threat and even buildings considered earthquake-resistant might be severely affected. As a matter of fact during the so-called "Christchurch sequence" around 70% of the central business district's (CBD) buildings turned out to be severely damaged and required to be demolished, in spite of the state-of-the-art New Zealand seismic building code and the stringent adoption and enforcement of this latter.

In this study we examine a large and representative set of numerical scenarios generated by means of physics-based simulations (PBS), in order to constrain the ground motion at short distances (within few kilometers range) by taking into account the rupture process, the seismic wave propagation and three-dimensional (3D) complex configurations. The experience gathered in the past years regarding 3D modelling of seismic wave propagation in complex alluvial basin (Guidotti et al., 2011; Smerzini and Villani, 2012) allowed us to enhance the choice of simulated scenarios in order to exhaustively explore the variability of ground motion and overcoming certain deficiency of the GMPEs and especially the insufficient number of records located close to the causative faults. All PBS presented in this study are carried out through the spectral element code SPEED (http://speed.mox.polimi.it).

The large metropolitan area of Beijing (China) is considered because of the (i) proximity with a well-known mapped fault system capable to trigger a severe earthquake, a (ii) relatively good description of the geotechnical characterization of the soil and a (iii) reliable reconstruction of the deep alluvial structure.

Focusing on the class of high-rise buildings and taking into account on one hand suitable fragility curves and on the other hand the aforementioned PBSs, seismic damage scenarios in the Beijing area will be produced and the variability of different damage states, as induced by a wide set of fault rupture scenarios with magnitude in the range 6.5-7.3 , will be explored.

Keywords: physics-based numerical simulations, damage scenario, fragility curves, high-rise buildings

1. INTRODUCTION

An accurate evaluation of seismic hazard, based on suitable approaches for earthquake ground motion prediction, is the key for the reliable assessment of seismic risk in large urban areas. However, the empirical approaches relying on Ground Motion Prediction Equations (GMPEs), that are most often used for this purpose, neglect the specific tectonic and geotechnical conditions in which the urban area lies and are poorly calibrated in the near-source region of large earthquakes, thus producing in many cases significant underestimations of the earthquake ground motion intensity.

In the recent years, stimulated by the increasing availability of computational resources, physics-based numerical simulations of earthquake ground motion including a full 3D seismic wave propagation model from the source to the site, have gained increasing interest so that they are expected to become, in near future, the most promising tool to generate ground shaking scenarios from future realistic earthquakes. In this work, the code SPEED - Spectral Elements in Elastodynamics with Discontinuous Galerkin (http://speed.mox.polimi.it/, Mazzieri et al. 2013), a certified high-performance open source code, developed by Politecnico di Milano, will be used to provide massive 3D broadband (i.e., usable

[1] Department of Mathematics, Politecnico di Milano, Italy, ilario.mazzieri@polimi.it

[2] Department of Mathematics, Politecnico di Milano, Italy, laura.melas@polimi.it

[3] Department of Civil and Environmental Engineering, Politecnico di Milano, Italy, chiara.smerzini@polimi.it

[4] Munich Re, Munich, Germany, mstupazzini@munichre.com

in the whole frequency range of interest for engineering applications) shaking scenarios in large urban areas.
The application of this state-of-art approach to several strategic urban areas worldwide (see review in Paolucci et al. 2014) is, therefore, of paramount importance to make this approach feasible and closer to the needs of seismic engineering applications. In this context, Munich RE funded a research activity with Politecnico di Milano between 2015 to 2017, having the objective of developing an advanced integrated probabilistic/deterministic procedure for seismic hazard assessment in large strategic urban areas, making use of 3D numerical physics-based ground shaking scenarios. In conjunction with this objective, the scope of the work presented in this paper was the generation of a wide set of 3D broadband physics-based ground shaking scenarios for the city of Beijing and its use for the assessment of seismic damage at urban scale.
Situated on a sedimentary basin, with its more than 20 million inhabitants, Beijing is one of the many megacities around the world highly exposed to the seismic threat. As a matter of fact, in the past thousand years, many destructive earthquakes have occurred in the area around Beijing, with magnitude varying from Mw 6 to Mw 6.5 (Gu et al. 1983).
Combining the aforementioned physics-based fault rupture scenarios with up-to-date fragility curves, seismic damage scenarios have been produced for the urban area of Beijing, with reference to the class of high-rise buildings, which represent an important proportion of assets at risk. The consideration of a wide set of physics-based ground shaking scenarios originating from an active fault passing through the city center with moment magnitude ranging from 6.5 up to 7.3 has allowed us to explore the variability of seismic damage to high-rise buildings and to investigate the role of near-fault ground motion.

1.1 Set-up of the 3D computational model for Beijing area

The 3D numerical model for the Beijing area encompasses the following features: i) the topography model; ii) a kinematic model for the seismic fault rupture; iii) the 3D basin model, defined from the depth of basement of sedimentary deposits and shear wave velocity profiles. For the elevation model, freely-available digital elevation dataset of CGIAR-CSI for the Beijing region has been extracted and downloaded from the website http://www.cgiar-csi.org (with a precision of roughly 90x90 m^2, for east-west and north-south directions around Beijing city). The seismic fault considered consists of the Shunyi-Qianmen-Liangxiang (SQL) fault, lying just through the downtown of Beijing (see superimposed line in Figure 2). The source is a quasi-vertical segmented fault (with dip angle of about 80°), consisting approximately of three main segments with different strike angles. The total length of the fault is about 90 km, considered therefore capable of producing up to magnitude 7.3 events.

To define the 3D velocity model, the sediments thickness derived from the digitalization of the map proposed in Gao et al. (2004) and the V_{S30} (shear wave velocity in the top 30 m) map of the area were used (see Figure 1 left and center). For the first layer at depths between 0 and 2 km, the shear wave velocity map (V_S) of Figure 1 (right) was used. The properties of the underlying bedrock layers (depth > 2 km) have been selected in agreement with Gao et al. (2004). The quality factor Q_S is estimated directly by the V_S values and is assumed to be proportional to frequency, for the target value $Q_S = V_S/10$ to be obtained at frequency f = 1 Hz.
The computational model, cf. Figure 2, was then set up by combining all information above and extends over an area of 70x70 km^2 down to 30 km depth, as illustrated in Figure 2. The conforming mesh has a size varying from a minimum of 150 m, on the top surface, up to 600 m at 4 km depth and reaching 1800 m in the underlying layers. The model consists of 859,677 hexahedral elements, resulting in approximately 160 million degrees of freedom, using a fourth order polynomial approximation degree. Considering a rule of thumb of 5 grid points per minimum wavelength for non-dispersive wave propagation in heterogeneous media by the spectral element approach, the model can propagate up to a maximum frequency f_{max} = 1.5 Hz.

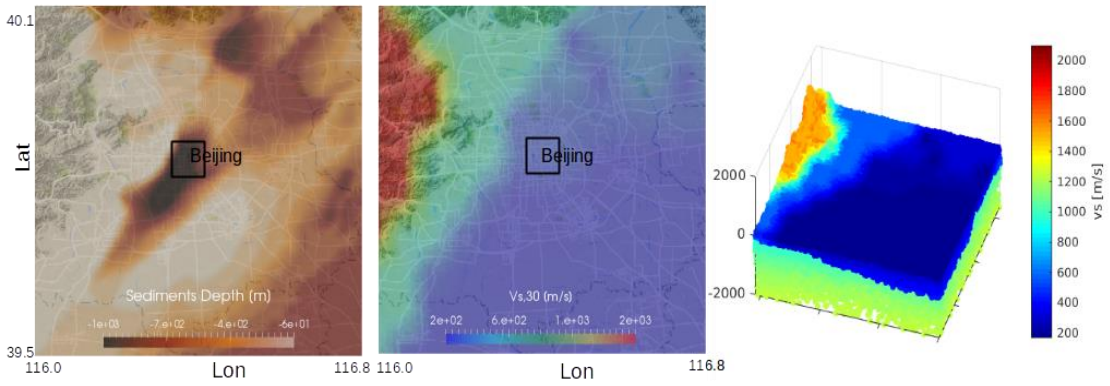

Figure 1. Sediment thickness (left), V_{S30} model (center) and $V_S(z)$ model (right) for the first layer 0-2 km.

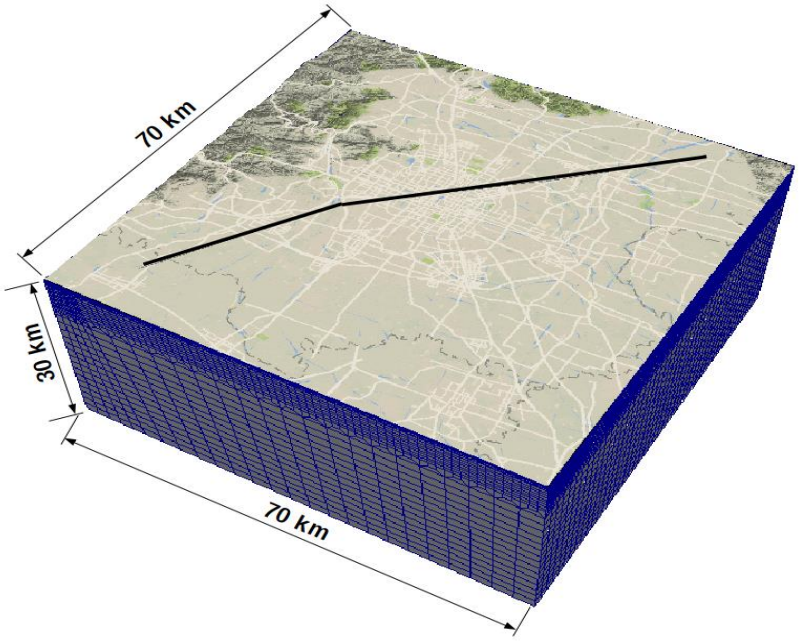

Figure 2. 3D computational model for the Beijing area. Black segments represent the trace of the considered Shunyi-Qianmen-Liangxiang fault.

1.2 Summary of simulated ground shaking scenarios

A total of 30 scenarios were simulated by varying the magnitude, from 6.5 up to 7.3, the kinematic slip distribution, the hypocenter location and the location of the rupture area. As regards the source model, to automatically construct N physically constrained slip distributions for a given fault and a given earthquake magnitude, a pre-processing tool has been devised taking into account joint probability distributions of the main kinematic parameters according to the broadband rupture generator proposed by Crempien and Archuleta (2015). Note that for each scenario, the rupture velocity follows the built-in scheme proposed in previously quoted paper, and the source time function is a simplified smoothed Heaviside function.

In order to model the non-linear soil behaviour of the soft soil deposits (V_{S30} <= 400 m/s) in the top 300 m, a simple Non-Linear visco Elastic (NLE) soil model has been considered (Stupazzini et al. 2009). A time step equal to 0.001 s has been chosen and a total observation time T = 60 s has been considered. The simulations were performed on the Marconi cluster at CINECA, Italy (http://www.cineca.it/en/content/marconi). Each simulation takes around 12 hours on 512 cores.

In Figure 3 (left column) we report the maps of the horizontal (geometric mean) Peak Ground Velocity

(PGV) obtained by computing the mean for all scenarios with magnitude Mw 6.5 (top), Mw 6.9 (middle) and Mw 7.3 (bottom). We remark that: i) these maps have been recovered by averaging the complete set of scenarios sharing the same magnitude, ii) only important urbanized areas are reported.
On the right-hand side of the same Figure we present the comparison with the ground motion prediction equation (GMPE) proposed by Cauzzi et al. (2015), estimated only for an average value of about 235 m/s (corresponding roughly to the average Vs30 of central Beijing) against the synthetic recordings. In order to present an average trend of the synthetics, these latter have been grouped adopting a sampling rate of 1 km: in a nutshell each receivers located at Rrupt +/- 0.5 km will be considered located at distance Rrupt, therefore the plot presents this quite distinctive aspect (Rrupt = closest distance to the fault rupture). The grey stars show the PGV simulated per receivers and scenarios, while the black dot simply represents the mean and the bar the dispersion around that value. For the sake of brevity no plot regarding one specific Vs30 is here proposed, nevertheless it is worth noting that our region of interest roughly correspond to the aforementioned 250 m/s and therefore we are confident of the relevance of this plot.
The numerical results obtained by SPEED are substantially in agreement with the proposed GMPE. However, synthetic scenarios produce higher PGVs in the proximity of the fault rupture. This has already been noted in many recent works (see e.g. Paolucci et al. 2014 and references therein), and may have a great impact on seismic hazard estimates, as standard GMPEs cannot account for such effects. Finally, we also report in Figure 4 some snapshots of the peak ground velocity wave field for a target scenario with magnitude Mw 7.3. It is possible to notice that the wave field propagates in the direction south-west to north-east and that higher values of PGV are obtained closed to the projection of the fault rupture on the surface, as to be expected.

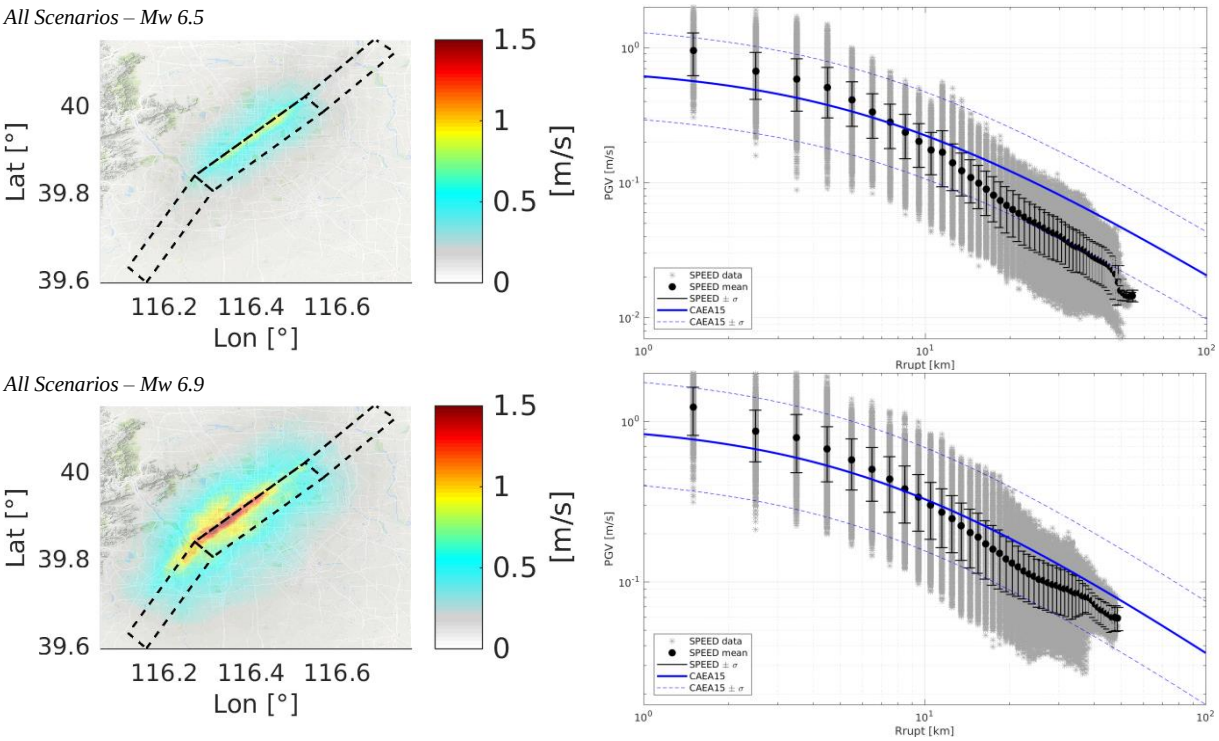

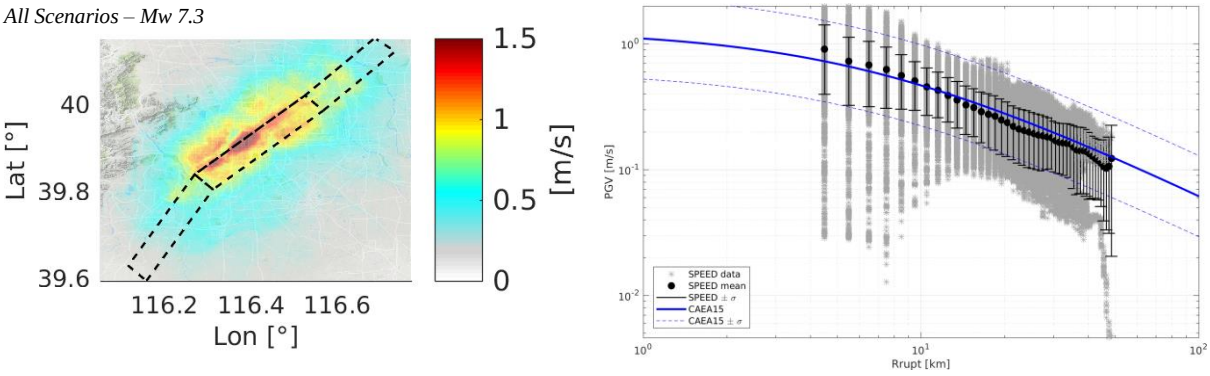

Figure 3. Left column: PGV maps obtained by averaging the scenarios at Mw 6.5 (top), Mw 6.9 (middle) and Mw 7.3 (bottom). Right column: comparison of GMPE by Cauzzi et al. (2015), (CAEA15) against PBSs. The grey stars show the PGV simulated per receivers and scenarios, while the black dot simply represents the mean and the bar the dispersion around that value.

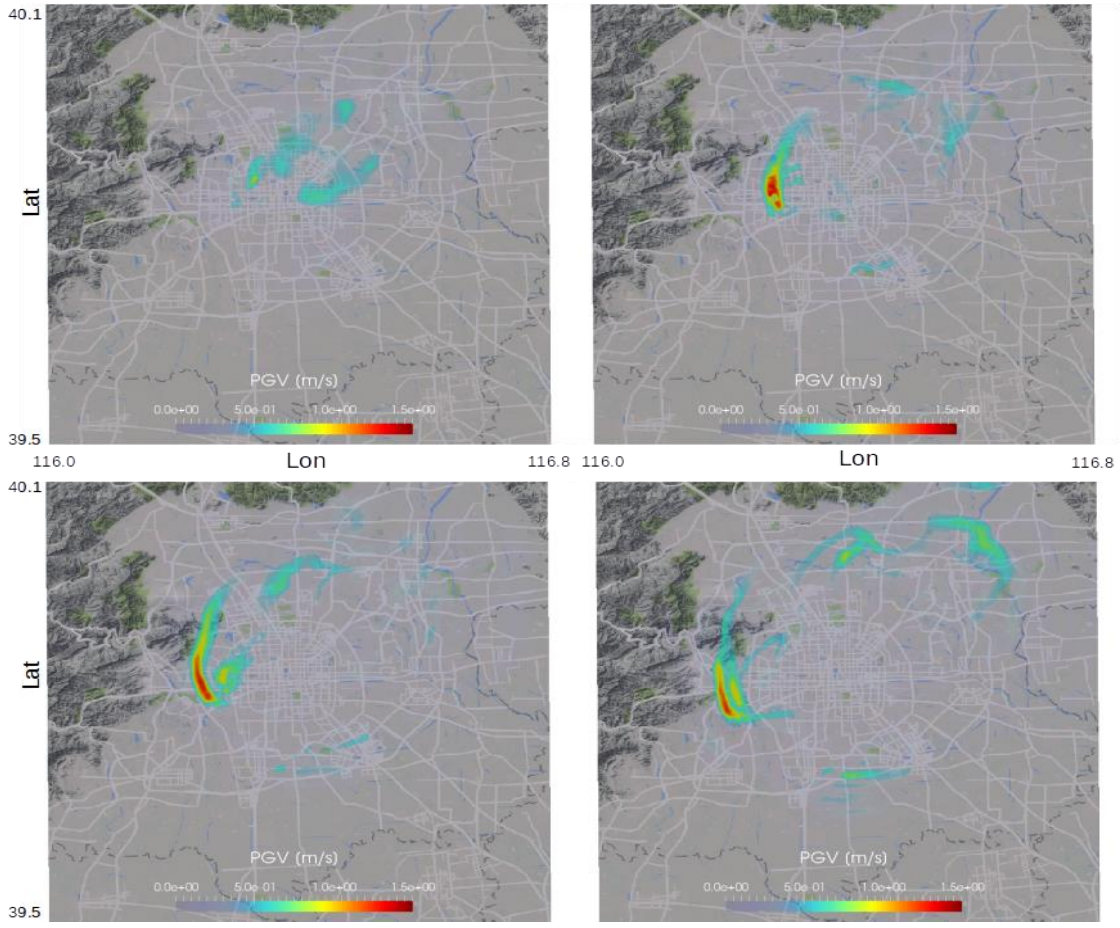

Figure 4. Snapshots of the PGV obtained for a scenario with Mw 7.3. Top-left: t = 8 s, top-right: t = 9 s, bottom-left: t = 10 s, bottom-right: t = 11 s.

1.3 Location of receivers and scenarios

As already shown in Figure 3, it was decided to sample each scenario with a special focus on points located in the metropolitan area of Beijing; we opted for a variable resolution grid (VRG) of receivers, having a minimum spacing of around 1.0km and thinning out as soon as the population density is decreasing.
Figures 5 and 6 illustrates the results in terms of response spectral displacement at 5% damping (SD) computed at vibration period T equal to 3 s, as obtained from four out of the 30 scenarios simulated along the SQL fault, which cross the central Beijing area striking in NE and EW directions, respectively. It is worth to note (i) the large difference of the SD observed between the two magnitude 6.5 events chosen, (ii) the significant expansion of the Beijing metropolitan area that is affected by very high values of ground motion at increasing magnitude and (iii) rather sharp gradient that characterizes all the maps presented here below.
Furthermore, thanks to the large number of synthetics recorded, it is also possible to appreciate on one hand the remarkable variability that our PBSs present for a given distance and on the other hand the almost systematic rapid decrease of the SD in terms of Rrupt.

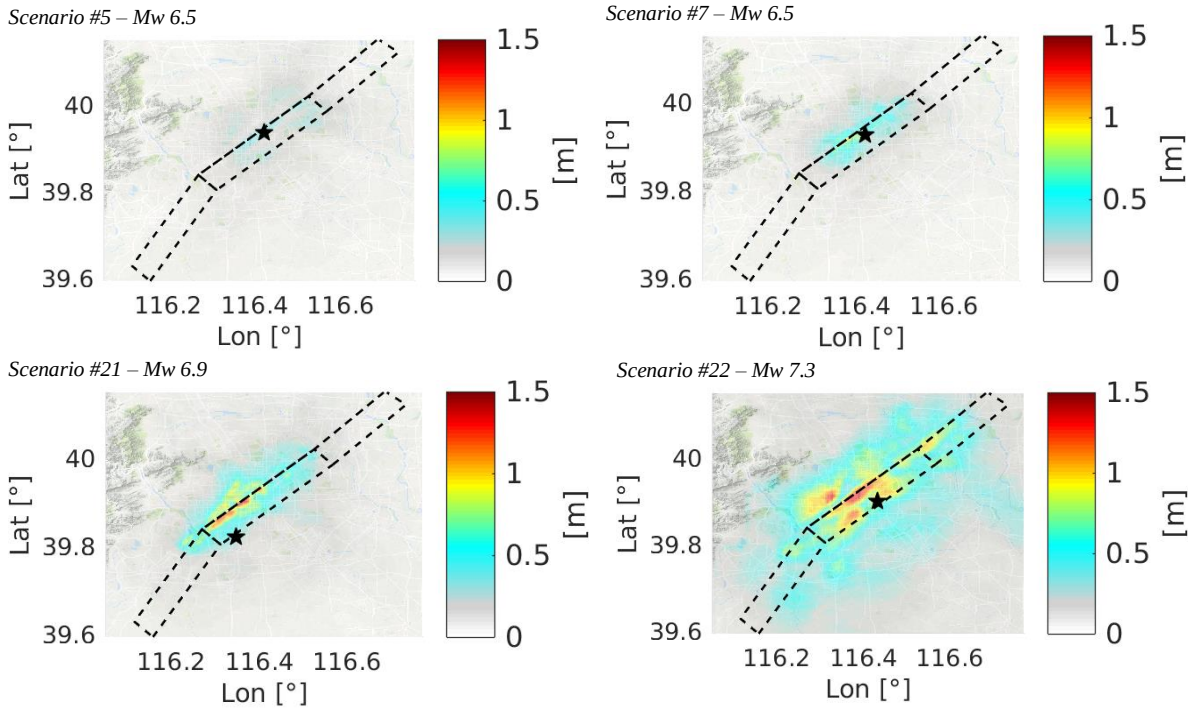

Figure 5. Spectral Displacement (SD) maps for T = 3s, as obtained for four different scenarios originating along the SQL fault.

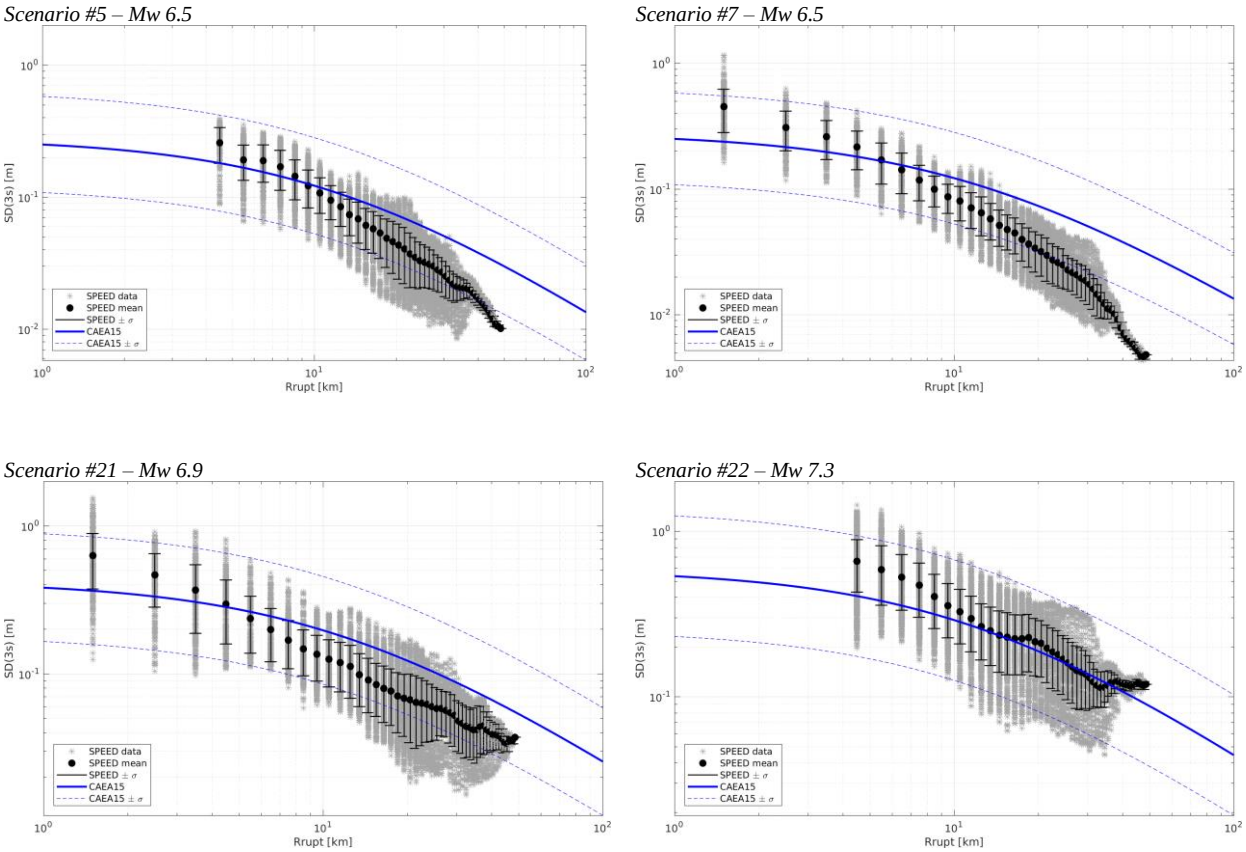

Figure 6. Spectral Displacement (SD) computed at T = 3s versus the closest distance to the fault rupture (Rrupt) : for each distance bin, grey stars denote the individual PBSs realizations, while filled black dots with bars represent the mean value and the corresponding standard deviation. The simulated data are compared against the prediction of Cauzzi et al. (2015) with a Vs30 = 235m/s.

2. HIGH RISE BUILDINGS

2.1 Building stock and fragility

In the present work we decided to focus on a class of buildings that represents nowadays a significant portion of the overall building stock in large metropolitan area in China and therefore it will clearly play a crucial role in deciding the resilience against earthquake of cities like Beijing in the future. Our target are the so called "super" high-rise buildings (whose height is over 100 m) that in spite of the many articles and researches available worldwide (e.g. Moehle et al., 2011; Kazantzi et al., 2014), seems to offer only few specific studies specifically focused on the Chinese building stock.
Indeed, Wu et al. (2013) presented a work, proposing a procedure to estimate the fragility curve of high-rise buildings based on spectral displacement. The authors highlighted that the dataset adopted refers to 56 high-rise and super high-rise Chinese buildings and to the corresponding seismic data, and that allowed them to investigate the relation between the maximum story drift angle and structural dynamic index. Finally, adopting the regulations of FEMA, which consists of four classes of structural performance, Normal Operation (NO), Immediate Operation (IO), Life Security (LS), Collapse Prevention (CP), they have been capable to create fragility curves associated to the aforementioned level of structural performance and they distinguished between two main categories: height over and below 200 meters (see Figure 7). According to FEMA the structural performance can be converted into an overall damage level as follow: NO = "Very Light", LS = "Light", IO = "Moderate" and CP = "Severe" as indicated in the FEMA273 (NEHRP guidelines for the seismic rehabilitation of buildings, 1997).

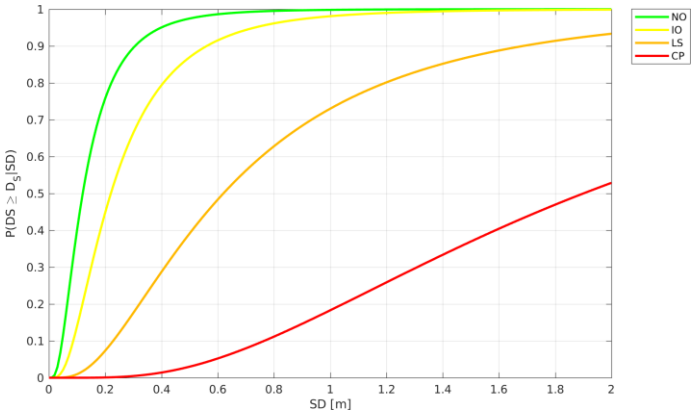

Figure 7. Fragility curves for buildings having a height below 200 meters and constructed with the so-called "low code" (From Wu et al., 2013).

Wu and coauthors also commented that "…above all, for the building below 200m, after SD is over 0.5 m, the exceeded probability of CP (Collapse Prevention) curves occur and develop rapidly […] when earthquake is small, the spectral displacement will be smaller, and NO (Normal Operation) exceeded probability will be small, which will accord with the 'Small Earthquake, No Collapse' requirement in the code." (Wu et al., 2013).
Our analyses suggest, as it will be shown in the following paragraph, that mostly the near-field of an earthquake, as to be expected, is controlling the probability of exceedance of a certain performance level and it might be argued that the distance from the fault and local geological condition, more than the magnitude itself, are the key parameters that must be taken into account.

2.2 Results of our analysis

Due to the fact that we are interested in investigating approximately 100 meters high-rise buildings, we decided to use the SD at 3 second as ground motion proxy. Out of that and adopting the aforementioned fragility curves we calculated the probability of different building performance levels and therefore in ultimate analysis the overall damage.
Figure 8 shows the probability of damage state (DS) being larger or equal than Life Security (LS) versus the closest distance to the fault rupture (Rrupt). Grey stars denote the P(DS≥LS) for each monitored points within the Beijing area, while filled black dots represent the mean of P(DS≥LS) at a given distance and the black bars represent the corresponding standard deviation. The LS damage state was chosen because the overall damage is classified as severe and therefore the building might be beyond economical repair.
Consistently with Figure 6, the probability of the LS performance level decreases significantly at Rrupt around 10 km but remains dangerously high at lower distances. The magnitude 7.3 scenario shows a similar overall trend, nevertheless the tendency is remarkably emphasized.
Finally the continuous and dashed blue lines represent the P(DS≥LS), adopting respectively the average and the +/- sigma SD as predicted by Cauzzi et al., (2015). It is worth to remark that the GMPE was used in a range of distances where very few empirical data are available.

Scenario #5 – Mw 6.5

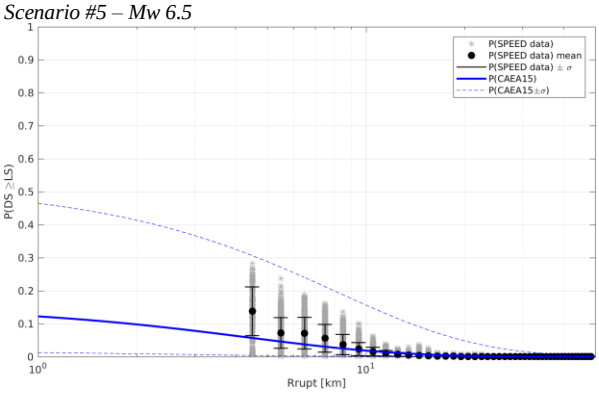

Scenario #7 – Mw 6.5

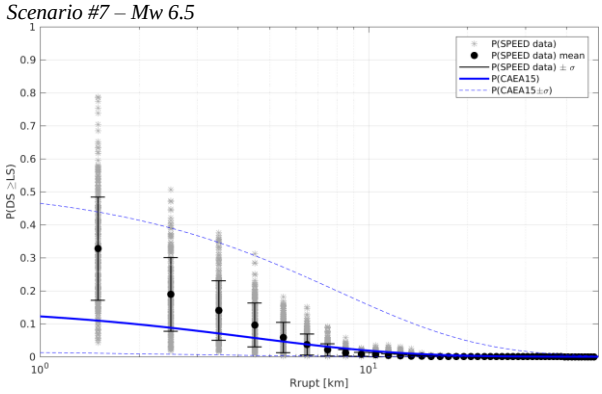

Scenario #21 – Mw 6.9

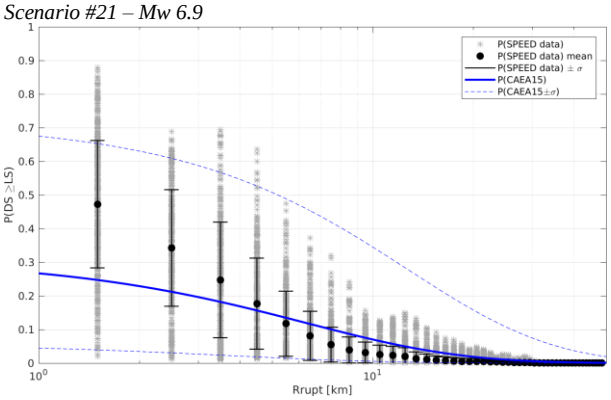

Scenario #22 – Mw 7.3

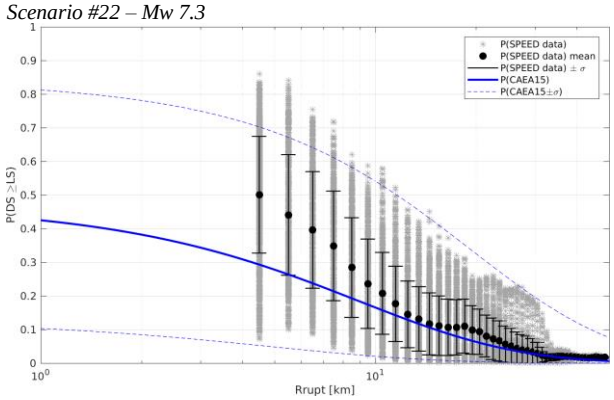

Figure 8. Normalized probability of damage state (DS) being greater or equal than Life Security (LS) versus the closest distance to the fault rupture (Rrupt). Grey stars denote the P(DS≥LS) for each monitored points within the Beijing area, while filled black dots represent the mean of P(DS≥LS) at a given distance and the black bars represent the corresponding standard deviation.

Figure 9 shows the results obtained out of the four already presented scenarios (#5, #7, #21 and #22) in terms of the probability of exceedance of the different Damage States. The black dots show the mean probability given a certain distance and the bars represent the standard deviation around the mean. It is worth to note the large dispersion around the mean value and once again the extremely rapid decrease of the probabilities associated to different damage state with respect to the Rrupt.

Finally in Figure 10 we selected different locations within the metropolitan area of Beijing and we assumed that a building like the one under investigation is located there. The different probability associated to the aforementioned FEMA performance levels, per scenario and location, are presented in terms of pie chart.
The overall tendency is clear: starting from scenario #5 (Mw 6.5) the dominating colors are white and green, respectively associated to damage states, No Damage (ND) and Normal Operation (NO), while the last scenario #22 (Mw 7.3) shows a predominance of the colors, yellow, orange and red. These are respectively associated to Immediate Operation (IO), Life Security (LS), Collapse Prevention (CP). Especially the last two levels are dangerous and should be carefully monitored.

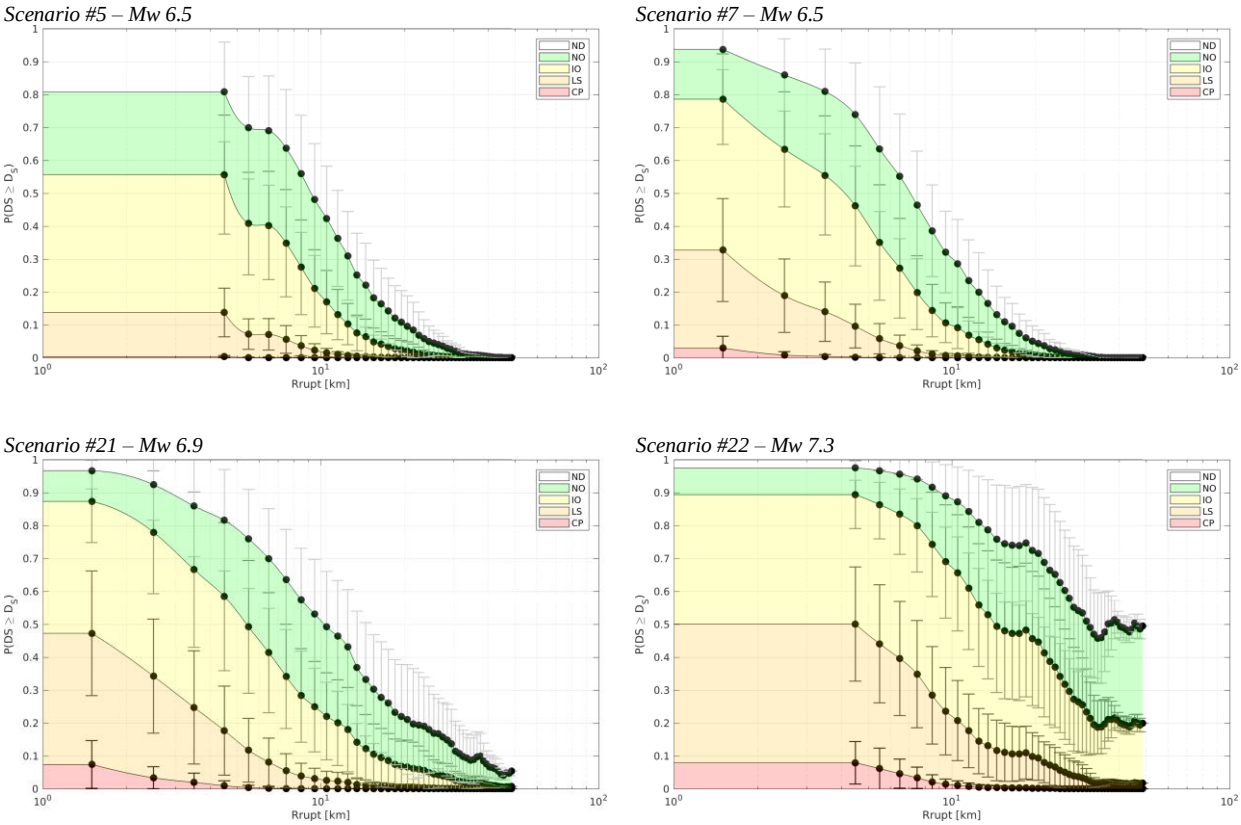

Figure 9. Normalized probability for all Damage States (DS) versus the closest distance to the fault rupture (Rrupt). The filled black dots represent the mean of $P(DS \geq D_S)$ at a given distance and the black bars represent the corresponding standard deviation. Consistently the different colors denote the $P(DS=D_S)$ (white: no damages – ND; green: very light damages, normal operation – NO; yellow: light damages, immediate operation – IO; orange: moderate damages, life security – LS; red: severe damages, collapse prevention – CP)..

	Location
1	Beijing Lang.&Cult. University
2	Feng Liang
3	International Trade Center
4	Natl. Conv. Center Grand Hotel
5	Haidian New Tech. Build.
6	Beijing Guangzhou Center Build.
7	China World Hotel
8	Building Amp Sky
9	China Natl. Offshore Oil Corp.
10	Peking Shopping Mall
11	Soubao Business Center
12	Changping District
13	Daxing District
14	Fangshan District
15	Fengtai East Street
16	Guanzhuang Village
17	Qiaoxi Street
18	Shijingshan District 1
19	Shijingshan District 2
20	Wangjing Street
21	Wukesong Area

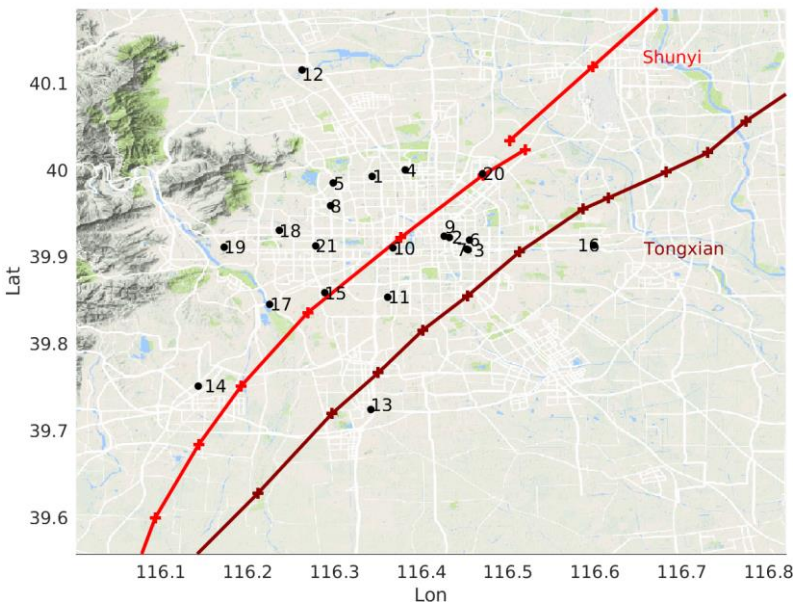

Figure 10. Location of the selected sites within the urban area of Beijing.

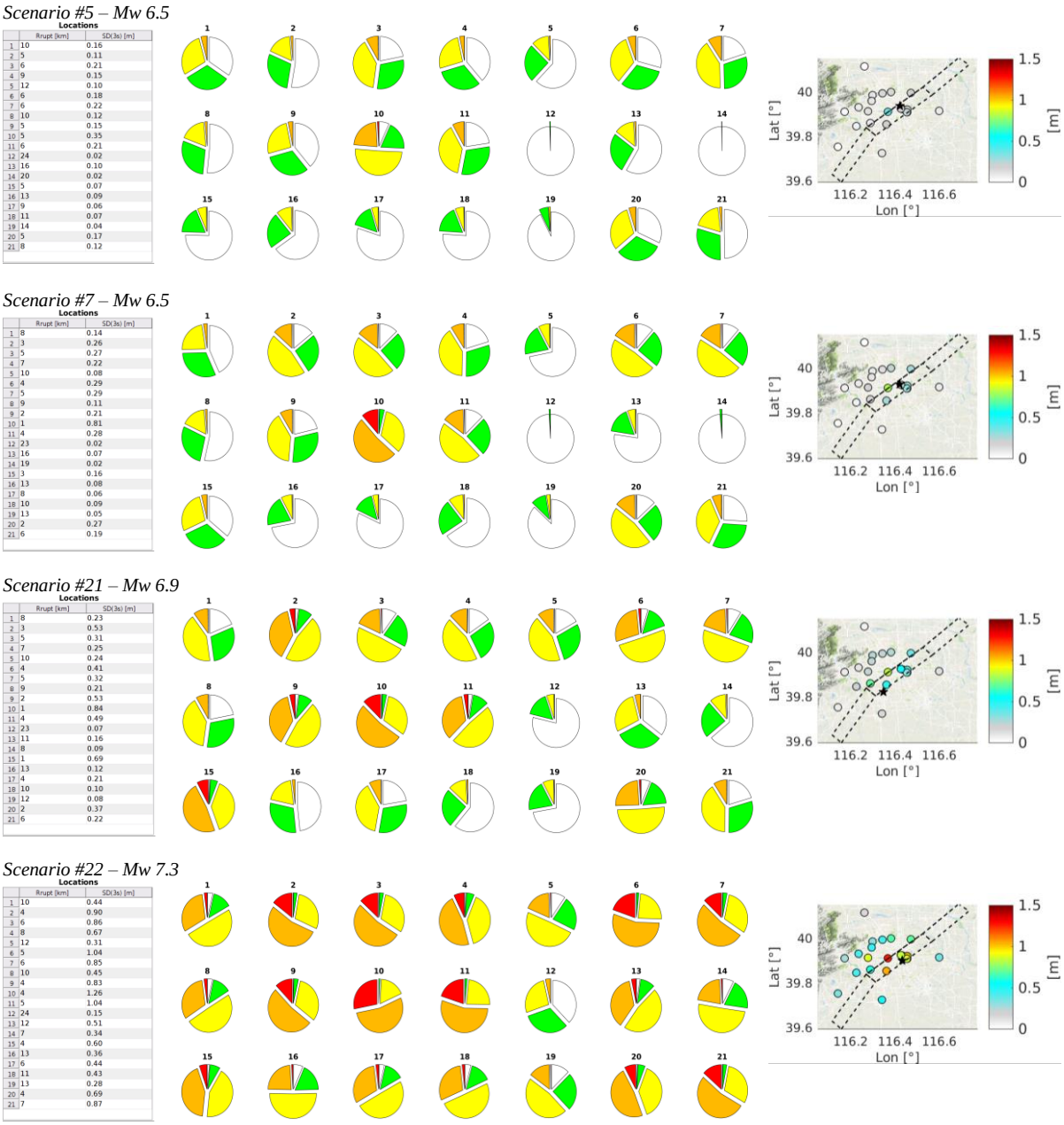

Figure 11. Left column: tables with information of the selected scenarios for all selected locations in Beijing. Middle column: pie charts for all damage states (DS) for each location in the urban area of Beijing. The different colors denote the P(DS=D_S) (white: no damages – ND; green: very light damages, normal operation – NO; yellow: light damages, immediate operation – IO; orange: moderate damages, life security – LS; red: severe damages, collapse prevention – CP). Right column: maps in terms of spectral displacement at T=3s for the locations in Beijing.

3. CONCLUSIONS

In this work we presented some preliminary analyses regarding a set of Physics-Based Scenarios that has been recently created. The aim is modelling as realistically as possible the ground shaking induced by a series of severe events occurring along the Shunyi-Qianmen-Liangxiang fault and affecting the Beijing metropolitan area. The most interesting novelty of the study is that we decided to perform a risk analysis adopting fragility curves available in literature for a class of buildings particularly relevant in China, the so-called "super" high-rise buildings, meaning with that the buildings with a

height higher than 100m. It is clear that only out of the dataset here presented and analyzed, no general indication can yet be drawn. Having said that, for a reliable prediction of the risk within a certain region, the careful characterization of the ground motion in the near-field of an earthquake remains of paramount importance. In fact, a systematic dangerously high probability of exceeding the performance levels "life security" and "collapse prevention" seems always to be restricted to locations having a distance from the fault ranging more or less from 10 up to 30 kilometers. Our analysis is at the moment restricted to a specific class of buildings, nevertheless our intention is to continue and investigating the seismic behavior of other building classes.

4. ACKNOWLEDGMENTS

We acknowledge the CINECA award under the LISA initiative, for the availability of high performance computing resources and support. This work was partially supported by the SIR Research Grant no. RBSI14VTOS funded by MIUR - Italian Ministry of Education, Universities and Research.

5. REFERENCES

Cauzzi C., Faccioli E., Vanini M., Bianchini A. (2015) Updated predictive equations for broadband (0.01 - 10 s) horizontal response spectra and peak ground motions, based on a global dataset of digital acceleration records. *Bulletin of Earthquake Engineering*, 13(6): 1587-1612.

Crempien J.G.F., Archuleta R.J. (2015) UCSB Method for Simulation of Broadband Ground Motion from Kinematic Earthquake Sources, *Seismological Research Letters*, 86 (1), 61-67.

Gao M., Yu Y., Zhang X., Wu J. (2004) Three-dimensional finite-difference modeling of ground motions in Beijing form a Mw 7 scenario earthquake. In *Proceedings of the 13th World Conference on Earthquake Engineering*, Paper No. 581.

Gu G., Lin T., Shi Z. (1983) Catalogue of earthquakes in China (1831AD-1969BC). Science Press, Beijing (in Chinese).

Guidotti R., Stupazzini M., Smerzini C., Paolucci R., Ramieri P. (2011) Numerical study on the role of basin geometry and kinematic seismic source in 3D ground motion simulation of the 22 February 2011 MW 6.2 Christchurch earthquake. Seismol Res Lett 82(6):767–782.

Kazantzi A., Vamvatsikos D., Porter K., Cho I.H.,(2014) Analytical vulnerability assessment of modern high rise RC moment-resisting frame buildings in the Western USA for the Global Earthquake Model, *Second European Conference on Earthquake Engineering and Seismology, Istanbul, 25-29 August 2014*.

Mazzieri I., Stupazzini M., Guidotti R., Smerzini C. (2013) SPEED: SPectral Elements in Elastodynamics with Discontinuous Galerkin: a non-conforming approach for 3D multi-scale problems, *International Journal for Numerical Methods in Engineering*, 95(12), 991–1010.

Moehle J.P., Bozorgnia Y., Jayaram N., Jones P., Rahnama M., Shome N., Tuna Z., Wallace J., Yang T., and Zareian F., (2011), Case Studies of the Seismic Performance of Tall Buildings Designed by Alternative Means, PEER Report No.2011/05, *Pacific Earthquake Engineering Research Center*, University of California, Berkeley.

Paolucci R., Mazzieri I., Smerzini C., Stupazzini M. (2014) Physics-based earthquake ground shaking scenarios in large urban areas, in *Perspectives on European Earthquake Engineering and Seismology, Geotechnical, Geological and Earthquake Engineering*, vol. 34, chap. 10, pp. 331–359, ed. Ansal, A., Springer.

Smerzini C., Villani M. (2012) Broadband numerical simulations in complex near field geological configurations: the case of the MW 6.3 2009 L'Aquila earthquake. Bull Seismol Soc Am 102(6):2436–2451.

Stupazzini M., Paolucci R., Igel H. (2009) Near-fault earthquake ground-motion simulation in Grenoble Valley by high-performance spectral element code. Bull Seismol Soc Am 99(1):286–301.

Wu, F., Wang M., Yang X.Y. (2013) Building Seismic Vulnerability Study for China High Rises. In *Advances in Civil and Industrial Engineering*. Applied Mechanics and Materials, vol. 353: 2301–2304.

MOX Technical Reports, last issues

Dipartimento di Matematica
Politecnico di Milano, Via Bonardi 9 - 20133 Milano (Italy)

38/2018 Domanin, M.; Gallo, D.; Vergara, C.; Biondetti, P.; Forzenigo, L.V.; Morbiducci, U.
Prediction of long term restenosis risk after surgery in the carotid bifurcation by hemodynamic and geometric analysis

40/2018 Chiappa, A.S.; Micheletti, S.; Peli, R.; Perotto, S.
Mesh adaptation-aided image segmentation

39/2018 Ferro, N.; Micheletti, S.; Perotto, S.
Density-based inverse homogenization with anisotropically adapted elements

37/2018 Bonaventura, L.; Della Rocca A.;
Convergence analysis of a cell centered finite volume diffusion operator on non-orthogonal polyhedral meshes

32/2018 Dal Santo, N.; Deparis, S.; Manzoni, A.; Quarteroni, A.
An algebraic least squares reduced basis method for the solution of nonaffinely parametrized Stokes equations

34/2018 Laurino, F.; Coclite, A.; Tiozzo, A.; Decuzzi, P.; Zunino, P.;
A muliscale computational approach for the interaction of functionalized nanoparticles with the miscrovasculature

35/2018 Possenti, L.; Casagrande, G.; Di Gregorio, S.; Zunino, P.; Costantino, M.L.
Numerical simulations of the microvascular fluid balance with a non-linear model of the lymphatic system

36/2018 Agosti, A.; Ambrosi, D.; Turzi, S.
Strain energy storage and dissipation rate in active cell mechanics

31/2018 Quarteroni, A.
The role of statistics in the era of big data: A computational scientist' perspective

30/2018 Ieva, F.; Palma, F.; Romo, J.
Bootstrap-based Inference for Dependence in Multivariate Functional Data